

Nanoporous Atomically Thin Graphene Membranes for Desalting and Dialysis Applications

Piran R. Kidambi,* Doojoon Jang, Juan-Carlos Idrobo, Michael S. H. Boutilier, Luda Wang, Jing Kong, and Rohit Karnik*

Dialysis is a ubiquitous separation process in biochemical processing and biological research. State-of-the-art dialysis membranes comprise a relatively thick polymer layer with tortuous pores, and suffer from low rates of diffusion leading to extremely long process times (often several days) and poor selectivity, especially in the 0–1000 Da molecular weight cut-off range. Here, the fabrication of large-area (cm²) nanoporous atomically thin membranes (NATMs) is reported, by transferring graphene synthesized using scalable chemical vapor deposition (CVD) to polycarbonate track-etched supports. After sealing defects introduced during transfer/handling by interfacial polymerization, a facile oxygen-plasma etch is used to create size-selective pores (≤ 1 nm) in the CVD graphene. Size-selective separation and desalting of small model molecules (≈ 200 –1355 Da) and proteins ($\approx 14\,000$ Da) are demonstrated, with ≈ 1 –2 orders of magnitude increase in permeance compared to state-of-the-art commercial membranes. Rapid diffusion and size-selectivity in NATMs offers transformative opportunities in purification of drugs, removal of residual reactants, biochemical analytics, medical diagnostics, therapeutics, and nano-bio separations.

Separation by dialysis is widely used across the entire spectrum of biochemical processes, e.g., to separate molecules like salts, small proteins, solvents, reducing agents, and dyes from larger macromolecules such as proteins, DNA, and polysaccharides, in buffer exchange, for purifying peptides, and in drug binding

Dr. P. R. Kidambi, D. Jang, Dr. M. S. H. Boutilier,
Dr. L. Wang, Prof. R. Karnik
Department of Mechanical Engineering
Massachusetts Institute of Technology
Cambridge, MA 02139, USA
E-mail: krpiran@mit.edu; karnik@mit.edu

Dr. P. R. Kidambi
Department of Chemical and Biomolecular Engineering
Vanderbilt University
Nashville, TN 37240, USA

Dr. J.-C. Idrobo
Center for Nanophase Materials Sciences
Oak Ridge National Laboratory
Oak Ridge, TN 37831, USA

Prof. J. Kong
Department of Electrical Engineering and Computer Science and
Research Laboratory of Electronics
Massachusetts Institute of Technology
Cambridge, MA 02139, USA

DOI: 10.1002/adma.201700277

studies.^[1,2] In dialysis, a sample solution and a dilute receiving solution (dialysate) are separated by a semipermeable membrane; the resulting concentration gradient leads to diffusion of molecules that are below the membrane cut-off size into the dialysate, whereas larger molecules/particles are retained.^[1] Conventional dialysis processes suffer from two major disadvantages: i) slow diffusion rates, and ii) poor selectivity close to the molecular weight cut-off ranges, greatly exacerbated in the lower molecular weight cut-off range of ≈ 0 –1000 Da.

The rate of diffusion of molecules across a dialysis membrane is inversely proportional to its thicknesses and also depends on porosity and tortuosity (i.e., zigzag flow path).^[1] Ideally, a dialysis membrane would permit rapid diffusion of solutes below the cut-off size, and block diffusion of all solutes above the cut-off.

The resistance that a membrane offers to transport is characterized by its permeance, i.e., rate of transport per unit membrane area per unit driving force. For a given pair of solutes to be separated, the ratio of the permeance of the two solutes, i.e., the selectivity, is also an important characteristic of the membrane. Generally, there is a trade-off between the selectivity and the permeance, which is well-known in gas separations^[3–5] but has not been adequately studied for dialysis-based separation.^[6–8]

For a membrane that permits a similar diffusivity (of the solute below the cut-off size) as that in bulk solution, and which does not interact significantly with the solute, permeance is equivalent to that of an unstirred bulk solution layer of effective thickness L_{eff} (see Transport equations discussion in Supporting Information) that is equal to the membrane thickness. The limiting case is an ultrathin membrane with high porosity, where L_{eff} would be on the order of the cut-off molecule size, on the order of nanometers. Practically, the limiting value is set by the thickness of boundary layers next to the membrane created due to limitations of stirring, but it is easily possible to achieve boundary-layer thicknesses on the order of ≈ 10 μm with conventional stirred cells.^[2,9] However, for practical membranes with a limited porosity (i.e., pores are only a fraction of membrane area), pore tortuosity, and molecule–membrane interactions that can hamper diffusion, the effective membrane thickness is often much higher than the actual membrane

thickness. Consequently, the permeance is low and the rate at which solutes can be removed from the sample solution is limited. For example, in a commercially available state-of-the-art dialysis membrane with 10–20 μm thickness, we observe an experimentally measured effective membrane thickness of ≥ 1 mm for small molecules below the molecular weight cut-off (see Figure S1, Supporting Information). These observations indicate that there is substantial room for reducing the processing time for dialysis by using a thin, selective membrane with L_{eff} on the order of ≈ 10 μm or less.^[7,8,10]

Here, atomically thin materials (2D materials) such as graphene (thickness ≈ 0.34 nm) offer the potential to realize the fundamental limit for physical thickness reduction in L_{eff} .^[11,12] In addition to atomic thinness, graphene also exhibits exceptional mechanical properties, i.e., few- μm^2 single layer can be suspended over supports and can withstand several atmospheres of pressure.^[13,14] The introduction of precisely engineered defects (narrow size distribution and high density) forms nanopores in these materials and allows for the development of nanoporous atomically thin membranes (NATMs).^[15–26] Due to their extreme thinness, NATMs with a narrow pore size distribution are hence expected to offer extremely high selectivity and permeance, thereby radically outperforming the current state-of-the-art polymer membranes.^[5,15] Furthermore, NATMs offer the potential to operate in solvents and under conditions where the performance of many polymeric membranes would deteriorate. However, we note that additional challenges such as fouling seen in polymeric materials are also relevant for 2D materials, but beyond the scope of the current study.

Here, we report on the synthesis of such NATMs for dialysis and desalting applications by transferring graphene grown via chemical vapor deposition (CVD) to polycarbonate track etched (PCTE) supports, followed by leakage sealing and selective pore creation (Figure 1). We observe clear evidence for size selectivity in graphene NATMs and ≈ 1 –2 orders of magnitude increase in permeance over the current state-of-the-art polymeric membranes, thereby offering significant advancement

for biochemical separations. To the best of our knowledge, this is the first demonstration of a fully functional large area (cm^2) atomically thin dialysis membrane.

Large-area NATMs (cm^2) were fabricated by polymer-free transfer of graphene on PCTE followed by leakage sealing and pore creation (Figure 1).^[16–18] First, monolayer CVD graphene grown on polycrystalline Cu foil was pressed against a PCTE support membrane with 200 nm pores. The Cu was subsequently etched to yield a polymer-free layer of graphene on PCTE. Scanning electron microscopy (SEM) of graphene on a PCTE support membrane (Figure 2A) indeed shows the majority of the 200-nm PCTE pores covered by suspended graphene (dark circles). However, the transfer process introduces few large tears in the graphene (Figure 2A), which are subsequently sealed using interfacial polymerization (IP, see Figures 1 and 2B,C). During IP, the graphene–PCTE stack is sandwiched between an aqueous solution of hexamethylene diamine in deionized water and an organic solution of adipoyl chloride in hexane (Figure 2B).^[17] Only in areas where the graphene is damaged/torn do the two solutions contact each other to form nylon 6,6 plugs that effectively seal the tears (Figure 1).^[17] Figure 2C shows an image of graphene (dark square) on a PCTE support after such defect sealing. The PCTE regions subjected to IP can be identified by the white clamp ring edge on graphene (see Figure 2C, superimposed dotted red line).

We use a diffusion cell (Figure 2D) to probe diffusive transport of ions and small molecules across the synthesized membranes. Transport across the synthesized membranes could arise from i) large tears in the graphene giving rise to nonselective transport (before sealing with IP), ii) nanopores in the graphene that give rise to selective transport, iii) transport through the polymer plugs formed by IP, and iv) combinations of the above. Diffusive flux across the synthesized membranes is normalized with respect to the flux across the bare PCTE membrane (see Figure 2E) for different model solutes: L-Tryptophan (L-Tr, ≈ 0.7 – 0.9 nm, 204 Da), Allura Red Dye (≈ 1 nm, 496 Da), Vitamin B12 (≈ 1 – 1.5 nm, 1355 Da),

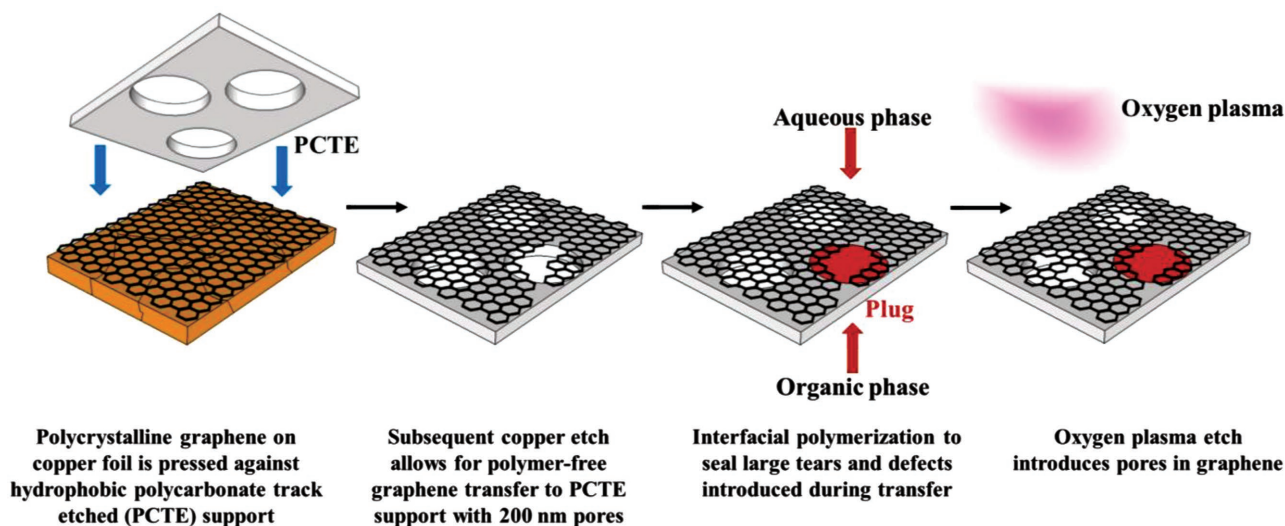


Figure 1. Synthesis of nanoporous atomically thin membranes (NATMs). Schematic overview of the process to synthesize large-area NATMs from CVD graphene grown on Cu foil.

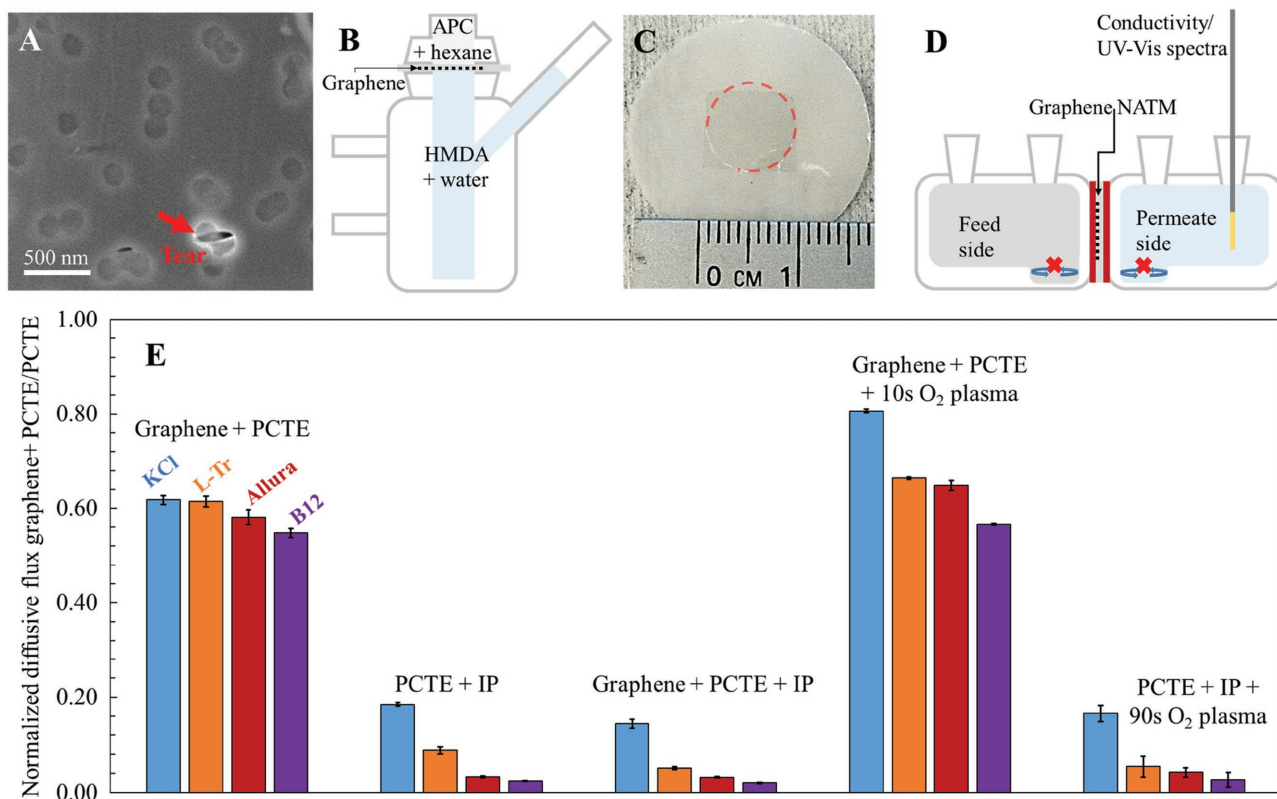


Figure 2. Probing transport across NATMs. A) SEM image of graphene on a PCTE support membrane. The dark circles indicate the 200 nm PCTE pores covered by graphene. Also seen in the image are tears in the graphene introduced during transfer. B) Schematic of the setup used for sealing tears in the graphene membrane using interfacial polymerization (IP). C) Photograph of graphene (dark square) on PCTE support membrane after IP. The region over which IP was performed can be identified by the white clamp ring edge on graphene. The dotted red line traces the edge of the area subjected to IP. D) Experimental setup used to measure the diffusive flux. E) Diffusive flux normalized with respect to bare PCTE support membrane for different membranes and solutes. Error bars indicate one standard deviation.

Lysozyme ($\approx 3.8\text{--}4$ nm, 14300 Da), and KCl (hydrated K^+ and Cl^- ions ≈ 0.66 nm).

After transfer of graphene on PCTE (Graphene + PCTE), we observe a decrease in flux of all solute species compared to bare PCTE, but significant flux remains and there is no observed selectivity, i.e., the normalized diffusive fluxes are: KCl ($\approx 62\%$), Allura Red ($\approx 58\%$), L-Tryptophan ($\approx 61\%$), and Vitamin B12 ($\approx 55\%$), with error bars showing standard deviation over triplicate measurements. Similar normalized fluxes compared to PCTE for KCl and Allura Red indicates similar transport pathways for ≈ 0.66 and 1-nm species, i.e., high structural quality of graphene with negligible sub-nanometer defects,^[27] thereby indicating large tears/defects from transfer/handling are the primary modes of transport.^[28] After sealing these large tears using IP, we find that fluxes for all species decrease significantly (Graphene + PCTE + IP) indicating that the IP successfully blocks nearly all large tears effectively, and that the remaining high quality graphene areas do not allow transport. A control experiment with interfacial polymerization on a bare PCTE support (PCTE + IP) also shows similarly reduced transport for all species, confirming the effectiveness of the sealing plugs. A small amount of KCl transport is observed for both Graphene + PCTE + IP and PCTE + IP (control), which we attribute to leakage of KCl through the IP plugs.

Having confirmed effective sealing of large tears in graphene, we now proceed to introduce size-selective pores by a facile oxygen plasma^[29] etch on the PCTE + Graphene + IP membranes. We qualitatively monitor the formation of defects in the graphene via Raman spectroscopy between each 15 s oxygen plasma etch increments on graphene transferred to SiO_2 (300 nm)/Si wafer. As seen in **Figure 3A**, the Raman spectrum for the starting material (0 s oxygen plasma) shows a fingerprint corresponding to monolayer graphene with 2D (≈ 2700 cm^{-1}) and G (≈ 1600 cm^{-1}) peaks but a barely noticeable D peak (≈ 1350 cm^{-1}), indicating the high structural quality^[30] of the graphene. This result is consistent with observations of similar diffusive transport rates for all species (Figure 2E, Graphene + PCTE), and contrasts with mild selectivity between KCl and Allura Red observed for graphene with nanometer-scale pore defects.^[18,31] After 15 s of plasma exposure, a huge increase in the D peak and an emergence of the D' peak (as a shoulder to the right of the G peak) are seen, indicating the creation of defects, and associated strain in the graphene lattice caused by damage from the oxygen plasma.^[30,32] Further increase in oxygen-plasma time increases the intensity of the D peak along with broadening and distinct changes in the 2D peak. These features are consistent with the formation of a mix of sp^2 and sp^3 bonds^[33–36] (see Figure S4, Supporting

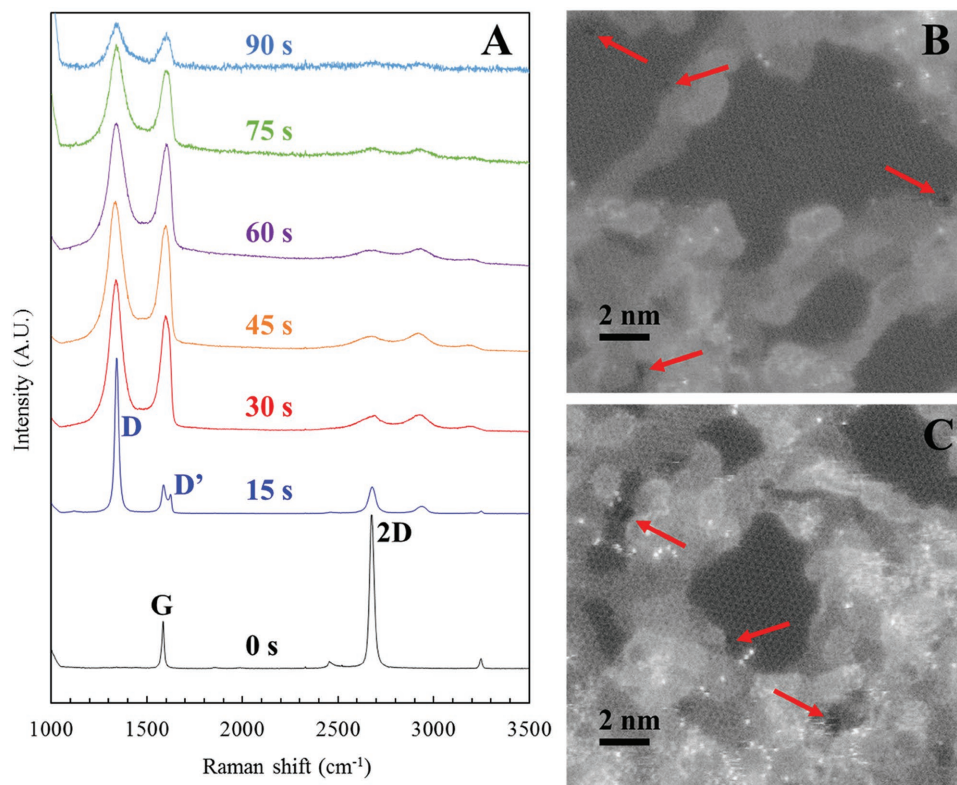


Figure 3. Nanopore creation by oxygen plasma. A) Raman spectra for graphene transferred to SiO₂ (300 nm)/Si wafer as a function of cumulative oxygen plasma exposure time. Increasing plasma exposure time causes the graphene to be more defective. B,C) High resolution scanning transmission electron microscopy (STEM) images corresponding to 75 s of oxygen plasma exposure time on suspended graphene shows nanoscale pores (red arrows) in the hexagonal graphene lattice.

Information) caused by: i) damage/attack from free radicals in the plasma, and ii) functionalization of dangling bonds with oxygen as reported by Zandiatashbar et al.^[32] An increase in oxygen-plasma time beyond 30 s does not cause significant change in the Raman spectrum except for a decrease in signal intensity, which could potentially arise from aggressive etching that leaves less material to interact with the laser.^[32] High-resolution scanning transmission electron microscopy (STEM) images of graphene with 75 s of plasma etch confirm the presence of sub-nanometer to nanometer-sized pores in the hexagonal graphene lattice (Figure 3B,C; red arrows indicate created pores; also see Figure S5, Supporting Information, for pore size distribution), consistent with the Raman spectra in Figure 3A. Transport measurements across graphene transferred to PCTE (without IP) and subjected to 10 s oxygen plasma etch (see Figure 2E, Graphene + PCTE + 10 s O₂ plasma) also show an increase in KCl flux compared to other molecules, further confirming the creation of selective nanopores in graphene in the absence of any polymer from IP.

Having confirmed the creation of sub-nanometer- to nanometer-sized pores in graphene, we proceed to measure transport properties across these pores for KCl, Allura Red, L-Tryptophan and Vitamin B12. **Figure 4A** shows the normalized diffusive flux for measurements performed on a single membrane that was repeatedly subjected to oxygen-plasma alternating with transport measurements. An increase in transport rates for all species is seen with increasing plasma time (Figure 4A),

while control experiments before and after a 90 s O₂ plasma etch on PCTE + IP membranes (see Figure 2E) do not show any increase in transport. However, the rate of increase in KCl transport with plasma treatment time is distinctly higher than that of L-Tr, Allura Red, and B12 (Figure 4A). These observations indicate the creation of a majority of sub-nanometer or nanometer-scale pores during successive oxygen-plasma etch pulses on the same membrane, along with perhaps a small contribution from enlargement of existing defects. Here, we note that a fraction of the transport is also attributed to tears in the graphene on the edges of the orifice due to declamping and re-clamping of the silicone rubber gaskets between each successive measurement on the same membrane.

To avoid potential damage to the membrane by repeated clamping and unclamping, experiments were performed with separate membranes, one for each oxygen plasma treatment time (Figure 4B). Although an increasing trend of KCl flux with increasing oxygen plasma treatment time was observed (Figure 4B), the flux of the other molecules was distinctly lower than that for the corresponding times when the membrane was repeatedly clamped and unclamped (Figure 4A). We observe the highest difference in flux ratios between KCl and other molecules for a plasma time of ≈60 s. For 90 s oxygen plasma time, we observe a noticeable increase in the flux of other molecules in addition to KCl (Figure 4B), indicating that larger pores that allow for transport of all molecules are being formed upon longer durations of exposure to plasma. The

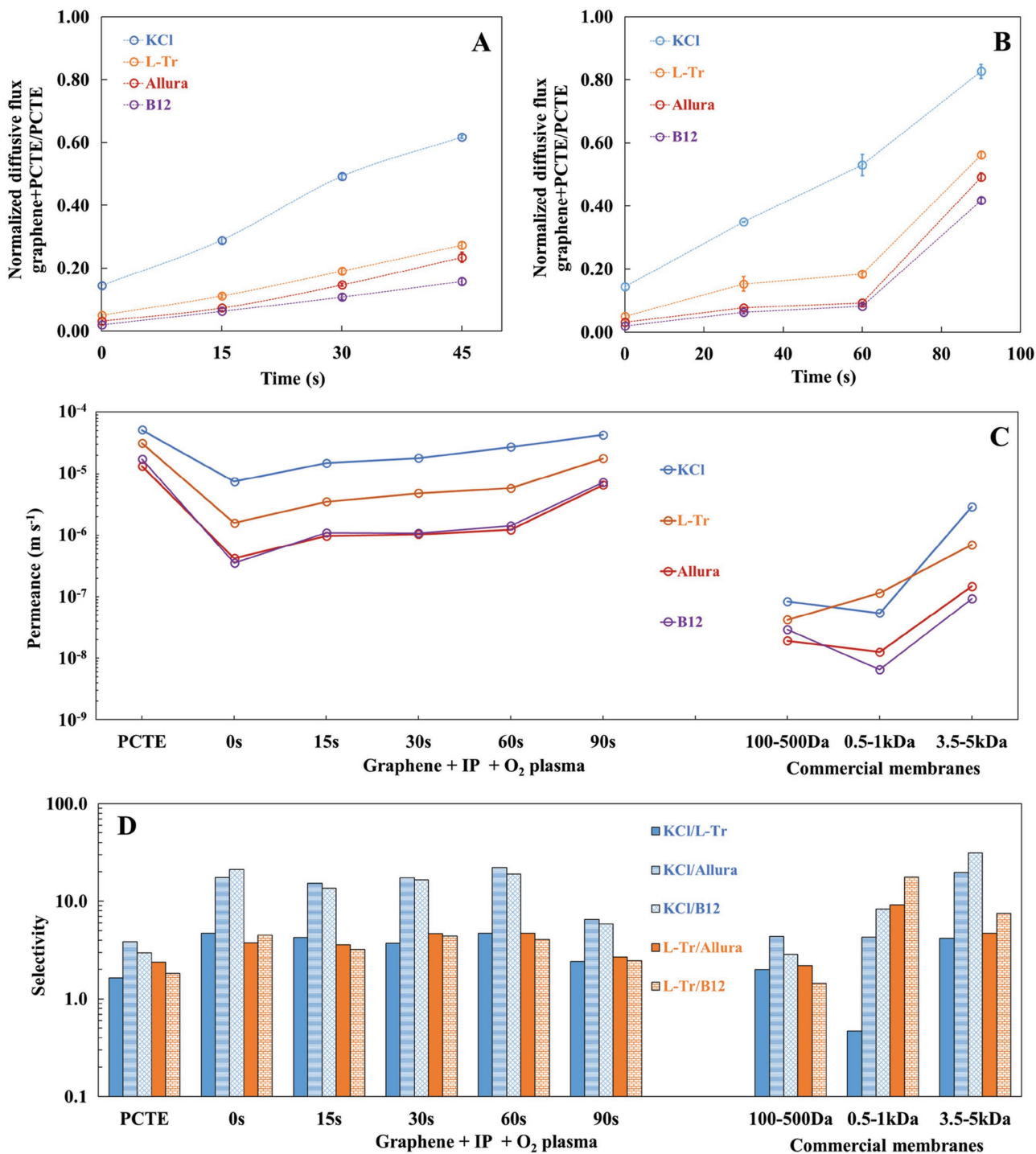


Figure 4. Selective pore creation in graphene membranes by oxygen plasma after sealing large tears via interfacial polymerization. Normalized diffusive flux as a function of O₂ plasma time (multiples of 15 s pulse) for PCTE + Graphene + IP + O₂ plasma with respect to bare PCTE for potassium chloride (KCl, K⁺, and Cl⁻ ≈0.66 nm), Allura Red (≈1 nm), L-Tryptophan (≈0.7–0.9 nm), and Vitamin B12 (≈1–1.5 nm) on A) the same membrane and B) across multiple membranes. Error bars show one standard deviation. C) Permeance (accounting for PCTE porosity of ≈10%) and D) selectivity (ratio of permeance of two species) for the synthesized NATMs and comparison with commercial membranes. See Figure S3 and S6 (Supporting Information) for selectivity as a function of permeance and permeance of NATMs without accounting for the PCTE porosity of ≈10%, respectively.

larger pores could be formed by enlargement of existing pores by plasma etching on pore edges or coalescence/merging of small pores as they grow. The oxygen plasma process can

hence be tuned to achieve the sizes required for separations and could potentially enable ultrafiltration applications based on NATMs.

We compare the performance of graphene NATMs with state-of-the-art commercial dialysis membranes with molecular weight cut-offs specified at 100–500, 500–1000, and 3500–5000 Da. To provide a direct comparison, we use the diffusion-driven transport experiments (Figure 4A,B) to compute the permeance (see experimental section):

$$P = \frac{J}{\Delta C} = \left(\frac{V \times \frac{dC}{dt}}{\Delta C \times A_{\text{effective}}} \right) \quad (1)$$

and selectivity (ratio of permeance of each diffusing species) for NATMs and commercial membranes (Figure 4C,D and Figure S3, also see Membrane transport model in the Supporting Information). We observe at least 1–2 orders of magnitude higher permeance for NATMs (Figure 4C, an effective area of 10% is used to compute graphene permeance) and distinctly higher selectivity (15–20) for KCl/Allura and KCl/B12 separations compared to the commercial membranes with 100–500 and 500–1000 Da cut-off, while only the 3500–5000 Da membrane shows slightly higher selectivity (Figure 4C,D; and Figure S3, Supporting Information). Further, the graphene NATMs show an increase in permeance with increasing oxygen plasma time (Figure 4C and Figure S6), while selectivity also increases for KCl/L-Tr and KCl/B12 separations (Figure 4D and Figure S3). These results suggest that graphene NATMs offer a significant advance for desalting, dialysis, and small molecule separation applications, particularly in the lower molecular weight cut-off ranges of 100–500 Da.

Finally, we demonstrate size selective separation of small molecules and proteins using the 60 s oxygen plasma etched NATMs (Figure 5), i.e., separation of salt and small molecules by dialysis. For the separation experiment, 7 mL aqueous solutions of KCl and L-Tryptophan (Figure S2A, Supporting Information), KCl and Vitamin B12 (Figure S2B, Supporting Information), and KCl and Lysozyme (Figure S2C, Supporting Information) were placed on the feed side of the diffusion cell (Figure 5A) and

their concentrations were monitored as the permeate side was continuously flushed with deionized water circulated from a large reservoir (≈ 70 L).

In all cases, the concentration of KCl drops rapidly following an exponential fit (Figure S2, Supporting Information), indicating rapid clearance by diffusion across the membrane. Further, the transport of L-Tr (≈ 0.7 – 0.9 nm, Figure 5B; and Figure S2A, Supporting Information) is seen to be greater than that of Vitamin B12 (1–1.5 nm, Figure 5B; and Figure S2B, Supporting Information), consistent with the observations of normalized diffusive flux for individual species in Figure 4A,B. These observations indicate that the majority of the pores created by the oxygen plasma pulsing process are indeed in the 0–1-nm size range. Many practical applications of desalting however, involve molecules much larger than 1 nm, e.g., proteins, DNA, polysaccharides. They are hence expected to be retained in fractions much larger than for Vitamin B12 by these graphene NATMs. The NATM indeed completely blocks transport of even small proteins such as Lysozyme (≈ 4 nm, 14 300 Da) indicating the absence of defects larger than ≈ 4 nm. Based on these observations we suggest that facile oxygen-plasma pulsing provides a simple way to realize NATMs that can be used for desalting, dialysis, and small molecular separation applications, specifically in the 0–1000 Da range.

Future research efforts toward increasing the support porosity, better leakage sealing approaches, and controlling pore size, along with membrane manufacturing methods compatible with roll-to-roll synthesis of high quality graphene will enable progress in this field. We note that the graphene permeance estimated here is a lower bound, and further improvements should be possible with design of appropriate supports, and with vigorous stirring (see membrane transport model in the Supporting Information). Although many separations require large-area membranes, we note that many lab-scale dialysis applications involve small volumes. The centimeter-scale membranes reported here are already useful for some of these practical separations.

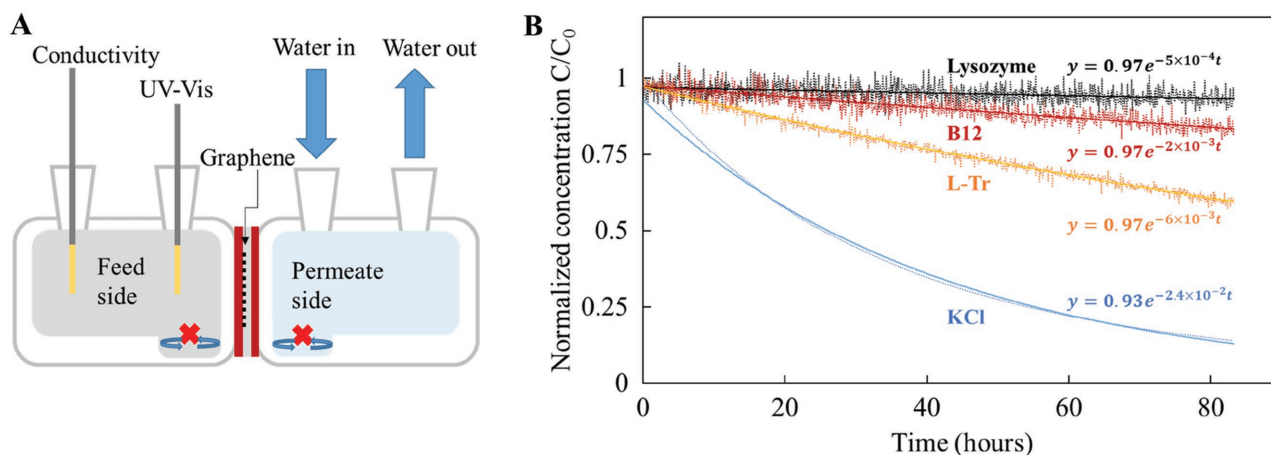


Figure 5. Size-selective separation using NATMs. A) Schematic of setup for separation experiment. B) Size-selective separation of KCl (≈ 0.66 nm) from model small molecules L-Tryptophan (≈ 0.7 – 0.9 nm), Vitamin B12 (≈ 1 – 1.5 nm), and Lysozyme (≈ 3.8 – 4 nm) using PCTE + Graphene + IP + 60 s O_2 plasma membrane. Conductivity and UV-vis spectra were measured on the feed side of the membrane for each molecule and KCl separately as shown in Figure S2 (Supporting Information). The solid lines denote the exponential fit to normalized concentrations (C/C_0). Note x-axis is plotted in hours but Figure S7 (Supporting Information) shows time in S.I. units of seconds.

In conclusion, we demonstrated atomically thin membranes with size-selective nanopores, formed using a facile and scalable process, for desalting, dialysis, and small molecule separations. The NATMs potentially offer 1–2 orders of magnitude improvement in permeance over commercially available state-of-the-art dialysis membranes in the 0–1000 Da range. Our work demonstrates the potential for use of 2D materials such as graphene in novel applications beyond electronics, and suggests that they could offer transformative improvements to separate molecules like salts, small proteins, solvents, reducing agents, and dyes from larger macromolecules such as proteins, DNA, and polysaccharides, in buffer exchange, for purifying peptides, and in drug binding studies.

Experimental Section

Graphene Growth: Graphene was synthesized by CVD on copper foil.^[37,38] Cu foil (JX Holding HA, 18 μm, 99.9%) was sonicated for 90 s in 15% HNO₃ to remove contaminants and oxides from the Cu surface and then washed in deionized water and finally dried in nitrogen. A hot-walled tube furnace was used to anneal the foil at growth temperature for 60 min in 60 sccm H₂ at ≈1.14 Torr. Graphene growth was performed by adding CH₄ (3.5 sccm ≈1.14 Torr) to H₂ at 1000–1050 °C for 30 min followed by 30 min of 7 sccm CH₄ (≈1.8 Torr) and 60 sccm H₂. After growth the foil was quench-cooled in the growth atmosphere.

Graphene Transfer, Interfacial Polymerization, and Pore Creation: For a polymer-free transfer, the side of Cu foil in contact with the quartz tube during CVD was pre-etched in ammonium persulfate (Transene APS-100) for 5 min to remove the graphene. CVD graphene on the side facing away from the quartz tube was pressed against PCTE support membranes with ≈10% porosity, 10 μm thickness (Sterlitech Inc., non-PVP coated, hydrophobic), and 200 nm diameter cylindrical pores, and the remaining Cu foil was completely etched. The graphene + PCTE stack was rinsed multiple times in deionized water followed by isopropanol.^[16–18] For transfer to TEM grids, a drop of ethanol or isopropanol on graphene on Cu foil was used to create adhesion as the solvent evaporates and the Cu foil was subsequently etched as above.^[17]

Interfacial polymerization (IP) was performed as reported elsewhere^[17] (see Figure 2B) using hexamethylene diamine in water (aqueous phase) and adipoyl chloride in hexane (organic phase) to plug any large tears introduced during the transfer with nylon 6,6. Prior to IP, graphene transferred on to PCTE was heated for 12 hours at 105–110 °C to remove any water at the interface and promote better adhesion.

Oxygen plasma etching was performed in pulses (500 mTorr, 15 s with 120 s pause between each pulse) in a plasma cleaner (Harrick Plasma PDC-001, maximum power 30 W) to create pores in graphene after sealing tears with IP.

Characterization: SEM images of graphene on PCTE were obtained using a Helios Nanolab Dualbeam 600 in immersion mode and Raman spectra were acquired with a Horiba Raman spectrometer with a 532 nm source. STEM was performed in Nion UltraSTEMTM 100, operated at 60 kV^[39] at ORNL's Center for Nanophase Materials Sciences. The CVD graphene was transferred to gold 200 mesh Quantifoil Holey Carbon transmission electron microscope grids (Ted Pella, Inc.) with 1.2 μm diameter holes, as described in more detail in ref. [17].

Transport Measurements: All diffusion-driven flow measurements across graphene NATMs were performed in triplicate after mounting the graphene-PCTE stack between two side-by-side diffusion cells (Permegear Inc., 5 mm orifice, 7 mL volume) as shown in Figure 2D.^[17] The membrane was initially rinsed three times with ethanol (KOPTec 200 proof ethanol anhydrous) to facilitate wetting of pores and prevent air bubble formation. After ethanol rinsing, the membrane was rinsed five times with deionized water.

For measuring diffusion-driven transport of KCl, 0.5 M KCl in deionized water was filled on the feed side (see Figure 2D) and the increase in conductivity of permeate side deionized water was monitored using a conductivity probe (eDAQ-Isopod). The slopes of the curves were taken after steady flow was established from 600–900 s to

compute the normalized flux for KCl $\left(\frac{\text{flow rate across graphene + PCTE}}{\text{flow rate across PCTE}} \right)$.

For Allura Red AC (98%, Sigma-Aldrich), L-Tryptophan (99%, Alfa Aesar), Vitamin B12 (Cyanocobalamin >98%, Alfa Aesar), and Lysozyme (ultrapure grade, VWR International) 0.5–1 × 10^{−3} M concentration of the solute in 0.5 M KCl was introduced on the feed side and 0.5 M KCl solution was introduced on the dialysate side; increase in concentration of the diffusing molecules on the dialysate side was measured using a UV–vis spectrometer (Agilent-Cary 60). Differences between 710 nm the deionized water (reference wavelength), and 510 nm for Allura Red, 279 nm for L-Tryptophan, 360 nm for Vitamin B12, and 282 nm for Lysozyme, respectively were used to compute concentrations from UV–vis spectra. Both sides are vigorously stirred to minimize concentration polarization effects and the ratio of the slope of concentration increase as a function of time for graphene + PCTE to PCTE was used to compute

the normalized flux $\left(\frac{\text{flow rate across graphene + PCTE}}{\text{flow rate across PCTE}} \right)$.

Permeance was calculated using $\left(\frac{V \times \frac{dC}{dt}}{\Delta C \times A_{\text{effective}}} \right)$ where V is volume

of the diffusion cell, A_{effective} is the effective area of the NATMs (10% of the area of the 5 mm diameter orifice, since PCTE has a porosity ≈10%) and ΔC is concentration difference. Selectivity between diffusing species is computed by taking the ratio of their permeance.

Separation experiments were similar to diffusion experiments except both conductivity and UV–vis spectra were measured on the feed side to quantify decrease in concentrations (Figure 5A). Further, the permeate side was constantly flushed with deionized water recirculated from a reservoir with a volume of ≈70 L using a peristaltic pump and an over flow to return the water to the reservoir.

Commercial dialysis membranes 100–500 Da (Spectrum lab CE Spectra Por), 500–1000 Da (Spectrum lab CE Spectra Por), and 3500–5000 Da (Spectrum lab Spectra Por, dry biotech regenerated cellulose dialysis membrane) were also measured for comparison with NATMs using a similar method as for graphene.

Supporting Information

Supporting Information is available from the Wiley Online Library or from the author.

Acknowledgements

P.R.K. and R.K. designed the experiments and wrote the manuscript. P.R.K. performed the experiments. D.J. prepared samples for STEM. J.-C.I. and D.J. performed STEM imaging. All authors contributed to discussions. P.R.K. acknowledges the Lindemann Trust Fellowship. This work was supported by U.S. Department of Energy, Basic Energy Sciences, Award No. DE-SC0008059. STEM imaging was conducted as part of a user project through Oak Ridge National Laboratory's Center for Nanophase Materials Sciences (CNMS), which is a U.S. Department of Energy Office of Science User Facility. This work made use of facilities at the Center for Nanoscale Systems (CNS) at Harvard University, a member of the National Nanotechnology Infrastructure Network, supported by the National Science Foundation under NSF Award No. ECS-0335765 and the MRSEC Shared Experimental Facilities at MIT, supported by the National Science Foundation under Award No. DMR-1419807. L.W. and J.K. acknowledge FATE MURI Grant No. FA 9550-15-1-0514.

This manuscript has been authored by UT-Battelle, LLC under Contract No. DE-AC05-00OR22725 with the U.S. Department of Energy. The United States Government retains and the publisher, by accepting the article for publication, acknowledges that the United States Government retains a non-exclusive, paid-up, irrevocable, world-wide license to publish or reproduce the published form of this manuscript, or allow others to do so, for United States Government purposes. The Department of Energy will provide public access to these results of federally sponsored research in accordance with the DOE Public Access Plan (<http://energy.gov/downloads/doe-public-access-plan>).

Conflict of Interest

R.K. is a co-founder and has equity in a startup company aimed at commercializing graphene membranes.

Keywords

atomically thin membranes, dialysis and desalting, nanoporous graphene membranes, selective transport, sub-nanometer pores

Received: January 13, 2017

Revised: May 19, 2017

Published online:

- [1] J. G. Crespo, K.W. Böddeker, *Membrane Processes in Separation and Purification*, Springer, Dordrecht, The Netherlands, **1994**.
- [2] H. P. Gregor, P. F. Bruins, M. Rothenberg, *Ind. Eng. Chem. Process Des. Dev.* **1965**, *4*, 3.
- [3] L. M. Robeson, *J. Membr. Sci.* **2008**, *320*, 390.
- [4] K. Celebi, J. Buchheim, R. M. Wyss, A. Droudian, P. Gasser, I. Shorubalko, J.-I. Kye, C. Lee, H. G. Park, *Science* **2014**, *344*, 289.
- [5] S. P. Koenig, L. Wang, J. Pellegrino, J. S. Bunch, *Nat. Nanotechnol.* **2012**, *7*, 728.
- [6] A. Saito, H. Kawanishi, A. C. Yamashita, M. Mineshima, *High-Performance Membrane Dialyzers*, Karger Publishers, Basel, Switzerland, **2011**.
- [7] Q. Yang, X. Lin, B. Su, *Anal. Chem.* **2016**, *88*, 10252.
- [8] M. E. Warkiani, A. A. S. Bhagat, B. L. Khoo, J. Han, C. T. Lim, H. Q. Gong, A. G. Fane, *ACS Nano* **2013**, *7*, 1882.
- [9] D. M. Malone, J. L. Anderson, *AIChE J.* **1977**, *23*, 177.
- [10] D. Cohen-Tanugi, R. K. McGovern, S. H. Dave, J. H. Lienhard, J. C. Grossman, *Energy Environ. Sci.* **2014**, *7*, 1134.
- [11] J. S. Bunch, S. S. Verbridge, J. S. Alden, A. M. Van Der, J. M. Parpia, H. G. Craighead, P. L. Mceuen, J. S. Bunch, S. S. Verbridge, J. S. Alden, A. M. Van Der Zande, J. M. Parpia, H. G. Craighead, P. L. Mceuen, *Nano Lett.* **2008**, *8*, 2458.
- [12] A. K. Geim, K. S. Novoselov, *Nat. Mater.* **2007**, *6*, 183.
- [13] D. Cohen-Tanugi, J. C. Grossman, *Nano Lett.* **2012**, *12*, 3602.
- [14] L. Wang, C. M. Williams, M. S. H. Boutilier, P. R. Kidambi, R. Karnik, *Nano Lett.* **2017**, *17*, 3081.
- [15] K. Celebi, J. Buchheim, R. M. Wyss, A. Droudian, P. Gasser, I. Shorubalko, J.-I. Kye, C. Lee, H. G. Park, *Science* **2014**, *344*, 289.
- [16] M. S. H. Boutilier, C. Sun, S. C. O'Hern, H. Au, N. G. Hadjiconstantinou, R. Karnik, *ACS Nano* **2014**, *8*, 841.
- [17] S. C. O'Hern, D. Jang, S. Bose, J.-C. Idrobo, Y. Song, T. Laoui, J. Kong, R. Karnik, *Nano Lett.* **2015**, *15*, 3254.
- [18] S. C. O'Hern, C. A. Stewart, M. S. H. Boutilier, J.-C. Idrobo, S. Bhaviripudi, S. K. Das, J. Kong, T. Laoui, M. Atieh, R. Karnik, *ACS Nano* **2012**, *6*, 10130.
- [19] T. Jain, B. C. Rasera, R. J. S. Guerrero, M. S. H. Boutilier, S. C. O'Hern, J.-C. Idrobo, R. Karnik, *Nat. Nanotechnol.* **2015**, *10*, 1053.
- [20] C. J. Russo, J. A. Golovchenko, *Proc. Natl. Acad. Sci. USA* **2012**, *109*, 5953.
- [21] R. C. Rollings, A. T. Kuan, J. A. Golovchenko, *Nat. Commun.* **2016**, *7*, 11408.
- [22] S. Garaj, W. Hubbard, A. Reina, J. Kong, D. Branton, J. A. Golovchenko, *Nature* **2010**, *467*, 190.
- [23] A. T. Kuan, B. Lu, P. Xie, T. Szalay, J. A. Golovchenko, *Appl. Phys. Lett.* **2015**, *106*, 203109.
- [24] Y. Zhao, Y. Xie, Z. Liu, X. Wang, Y. Chai, F. Yan, *Small* **2014**, *10*, 4521.
- [25] C. Sun, M. S. H. Boutilier, H. Au, P. Poesio, B. Bai, R. Karnik, N. G. Hadjiconstantinou, *Langmuir* **2014**, *30*, 675.
- [26] J. Feng, K. Liu, M. Graf, M. Lihter, R. D. Bulushev, D. Dumcenco, D. T. L. Alexander, D. Krasnozhan, T. Vuletic, A. Kis, A. Radenovic, *Nano Lett.* **2015**, *15*, 3431.
- [27] P. R. Kidambi, R. A. Terry, L. Wang, M. S. H. Boutilier, D. Jang, J. Kong, R. Karnik, *Nanoscale*, **2017**, DOI: 10.1039/c7nr01921a.
- [28] S. C. O'Hern, M. S. H. Boutilier, J.-C. Idrobo, Y. Song, J. Kong, T. Laoui, M. Atieh, R. Karnik, *Nano Lett.* **2014**, *14*, 1234.
- [29] S. P. Surwade, S. N. Smirnov, I. V. Vlasiouk, R. R. Unocic, G. M. Veith, S. Dai, S. M. Mahurin, *Nat. Nanotechnol.* **2015**, *10*, 459.
- [30] A. C. Ferrari, D. M. Basko, *Nat. Nanotechnol.* **2013**, *8*, 235.
- [31] P. R. Kidambi, M. S. H. Boutilier, L. Wang, D. Jang, J. Kim, R. Karnik, *Adv. Mater.* **2017**, *29*, 1605896.
- [32] A. Zandiatashbar, G.-H. Lee, S. J. An, S. Lee, N. Mathew, M. Terrones, T. Hayashi, C. R. Picu, J. Hone, N. Koratkar, *Nat. Commun.* **2014**, *5*, 3186.
- [33] A. Merenda, E. des Ligneris, K. Sears, T. Chaffraix, K. Magniez, D. Cornu, J. A. Schütz, L. F. Dumée, *Sci. Rep.* **2016**, *6*, 31565.
- [34] A. Felten, A. Eckmann, J.-J. Pireaux, R. Krupke, C. Casiraghi, *Nanotechnology* **2013**, *24*, 355705.
- [35] W. S. Lim, Y. Y. Kim, H. Kim, S. Jang, N. Kwon, B. J. Park, J.-H. Ahn, I. Chung, B. H. Hong, G. Y. Yeom, *Carbon* **2012**, *50*, 429.
- [36] N. McEvoy, H. Nolan, N. Ashok Kumar, T. Hallam, G. S. Duesberg, *Carbon* **2013**, *54*, 283.
- [37] P. R. Kidambi, C. Ducati, B. Dlubak, D. Gardiner, R. S. Weatherup, M. Martin, P. Seneor, H. Coles, S. Hofmann, *J. Phys. Chem. C* **2012**, *116*, 22492.
- [38] P. R. Kidambi, B. C. Bayer, R. Blume, Z.-J. Wang, C. Baetz, R. S. Weatherup, M.-G. Willinger, R. Schloegl, S. Hofmann, *Nano Lett.* **2013**, *13*, 4769.
- [39] O. L. Krivanek, G. J. Corbin, N. Dellby, B. F. Elston, R. J. Keyse, M. F. Murfitt, C. S. Own, Z. S. Szilagyi, J. W. Woodruff, *Ultramicroscopy* **2008**, *108*, 179.